Numerical Simulation of Pressure Boundary Failure Accident in Lead Bismuth Eutectic-Supercritical Carbon Dioxide Printed Circuit Heat Exchangers

Authors: Huang, Mr. Xi, Zhang, Mr. Lixiang, Huang, Mr. Yuxin, Zhang, Mr. Kefan, Chen, Prof. Hongli, Chen, Prof. Hongli

Date: 2025-06-04T16:31:14+00:00

Abstract

Due to its excellent heat transfer performance and compact structure, the printed circuit heat exchanger (PCHE) has become the mainstream heat exchange equipment between the secondary circuit of the supercritical carbon dioxide Brayton cycle and the primary circuit of the lead-cooled fast reactor. During operation of the Lbe-SCO2 PCHE, the substantial pressure differential between the cold side (high-pressure S-CO2) and the hot side (atmospheric-pressure lead-bismuth eutectic), combined with the corrosive characteristics of the lead-bismuth eutectic, could lead to failure of the PCHE pressure boundary, potentially resulting in CO2 leakage into the primary circuit. This study used the CFD software ANSYS Fluent to numerically simulate PCHE pressure boundary failure accidents. The feasibility of the analysis method was verified by decomposing complex accident conditions into typical characteristic conditions for experimental simulation verification. The results show that during the accident transient process, pressure in the hot channel initially exhibits cyclic fluctuations, rising sharply within 0.1 ms and then gradually stabilizing, while pressure in the cold channel remains essentially unchanged at operating pressure. The simulation revealed that 15 ms after the accident, large quantities of carbon dioxide were detected at the inlet and outlet of the hot side, indicating a risk of secondary circuit working medium intrusion into the reactor.

Full Text

Preamble

Numerical Simulation of Pressure Boundary Failure Accident in Lead-Bismuth Eutectic-Supercritical Carbon Dioxide Printed Circuit Heat

Exchanger

Xi Huang,[1] Li-Xiang Zhang,[1] Yu-Xin Huang,[1] Ke-Fan Zhang,[1] and Hong-Li Chen[1],* [1]School of Nuclear Science and Technology, University of Science and Technology of China, Hefei, Anhui, 230026, China

Due to its excellent heat transfer performance and compact structure, the printed circuit heat exchanger (PCHE) has become the mainstream heat exchange equipment between the secondary circuit of the supercritical carbon dioxide Brayton cycle and the primary circuit of the lead-cooled fast reactor. During operation of the LBE-SCO_2 PCHE, the enormous pressure difference between the cold side (high-pressure S-CO_2) and hot side (atmospheric-pressure lead-bismuth eutectic), combined with the corrosion characteristics of lead-bismuth eutectic, could lead to PCHE pressure boundary failure, potentially resulting in CO_2 leakage into the primary circuit. This study employs CFD software ANSYS Fluent to numerically simulate PCHE pressure boundary failure accidents. The feasibility of the analysis methodology is verified by decomposing complex accident conditions into characteristic conditions for experimental validation. Results demonstrate that during the accident transient, pressure in the hot channel initially exhibits cyclic fluctuations, rising sharply within 0.1 ms before gradually stabilizing, while pressure in the cold channel remains essentially unchanged at operating pressure. Simulations reveal that 15 ms after the accident, large quantities of carbon dioxide are detected at the hot side inlet and outlet, indicating a risk of secondary circuit working medium intrusion into the reactor.

INTRODUCTION

The supercritical CO_2 (S-CO_2) Brayton cycle power generation system has become an ideal energy conversion solution for Generation IV nuclear reactors due to its significant advantages, including compact equipment size, high thermal efficiency, and operational flexibility [1]. The lead-cooled fast reactor (LFR), as one of the most promising reactor types among Generation IV reactors, with its compact structure, small volume, and excellent thermal efficiency, perfectly matches the advantages of the S-CO_2 Brayton cycle system [2].

The printed circuit heat exchanger (PCHE) offers high heat transfer capacity and small mass and size, making it the most widely used heat exchanger in the S-CO_2 Brayton cycle [3]. As the pressure boundary between primary and secondary circuits, the lead-bismuth eutectic (LBE)-S-CO_2 heat exchanger faces a significant pressure difference between liquid lead-bismuth and supercritical CO_2, making safety issues arising from pressure boundary failure and resulting leakage non-negligible. Potential pressure boundary failure in the heat exchanger will cause supercritical CO_2 on the cold side to leak into the hot side and pressurize the system, threatening the structural integrity of the heat exchanger itself and related boundary systems. It is necessary to evaluate boundary failure accidents to confirm their safety impact.

Currently, no direct experiments exist on contact between liquid lead-bismuth and carbon dioxide, and very few experiments have been conducted on contact between carbon dioxide and liquid metals. Jae-Hyuk Eoh et al. [4] conducted mixing experiments of S-CO_2 and sodium to analyze the mixing of the two substances due to PCHE heat exchanger boundary condition failure, obtaining reaction models for these substances and kinetic parameters for different reaction zones. Naoyuki Kisohara et al. [5] investigated the effect of S-CO_2 leakage from the PCHE of a sodium fast reactor (SFR) to the sodium pipeline on pressure increase and heat transfer performance in the primary circuit. Results showed that CO_2 leakage did not significantly affect the core and primary circuit boundary due to the small volume of single runners in the PCHE. Only studies of CO_2 exposure to sodium have been conducted, with no studies on LBE/Pb. Compared with SFRs with intermediate loops, boundary condition failure accidents in LFRs may directly affect core safety. The main difference between lead-bismuth eutectic and sodium is chemical stability; at operating temperatures, liquid lead-bismuth eutectic has relatively low chemical reaction activity and will not undergo vigorous chemical reactions with supercritical carbon dioxide.

Based on the ANSYS Fluent numerical simulation platform, this study aims to investigate the pressure wave propagation characteristics of a lead-bismuth eutectic-supercritical carbon dioxide (LBE-SCO_2) printed circuit heat exchanger (PCHE) under a boundary condition failure accident. By decomposing the accident characteristics, the complex accident scenario is divided into typical transient processes, and the reliability of the numerical model is verified by comparing with experimental data. The study focuses on the propagation characteristics and evolution laws of pressure waves in the piping system during the accident transient process and analyzes the leakage characteristics. The migration and diffusion behavior of the leaked working fluid in the circuit was preliminarily assessed to evaluate the risk of CO_2 leakage to the reactor core.

II. MODEL VALIDATION

The boundary failure accident in an LBE-SCO_2 printed circuit heat exchanger (PCHE) can be characterized as follows: a fracture occurs in the solid region between the cold and hot channels, creating a connection that allows high-pressure CO_2 to enter the low-pressure lead-bismuth eutectic (LBE) channel. When the accident occurs, high-pressure S-CO_2 flows into the hot channel, undergoes transcritical depressurization, and transitions from a supercritical to a gaseous state. The resulting pressure wave propagates through the liquid LBE. However, there is currently very limited information available for such design considerations.

For the boundary failure accident analyzed in this study, the following assumptions are adopted: • Supercritical carbon dioxide is chemically relatively inert at high temperatures and pressures. It is generally accepted that dry pure S-CO_2 fluids are stable at lower temperatures (<400 °C) and have a very low probability of reacting with metal parts in contact (pressure vessels, piping,

etc.) [6]. • The disappearance of surface tension in supercritical fluids eliminates the stratification phenomenon between liquid and gas phases [7]. When S-CO_2 comes into contact with liquid metals, the surface tension of the liquid metal plays a dominant role.

In this paper, the boundary failure accident characteristics are divided into the following two points, with corresponding experimental validations conducted to evaluate the feasibility of the simulation methodology: • Transcritical depressurization analysis of supercritical carbon dioxide • Pressure wave analysis of gas injection into liquid metal

A. Verification of the Supercritical Carbon Dioxide Transcritical Depressurization Model

To investigate the depressurization characteristics of S-CO_2, Gebbeken [8] performed depressurization experiments on the top of an S-CO_2 container, focusing particularly on flashing scenarios during pressure release. The study obtained comprehensive data on axial fluid temperature distribution, transient pressure evolution, and void fraction dynamics along the vessel's central axis, while systematically analyzing the influence of initial parameters on these characteristics. Wang et al. [9] conducted vessel depressurization experiments with S-CO_2 using nozzles of varying sizes under different initial temperature and pressure conditions. Their observations revealed that the initial temperature directly influences the occurrence of phase transition. Guo et al. [10] conducted experiments on the depressurization of industrial-scale pipelines with S-CO_2 and observed gas-liquid and gas-solid phase transition phenomena during the process.

In terms of numerical simulation, Ming et al. [11] established a transient characteristic model for S-CO_2 discharge inside a pressure vessel based on Modelica. The program's flow rate and pressure calculation results were in good agreement with experimental data. Liu [12] used Fluent to conduct numerical simulations and analyses of the near-field jet and far-field shockwave structure of S-CO_2 leakage, utilizing the PR equation of state. Li [7] conducted a numerical simulation study on the free expansion jet process in small-scale supercritical leakage near-field using a self-developed two-step Lax-Wendroff (L-W) algorithm, with parallel experimental data comparison for validation. The thermodynamic parameters of CO_2 were calculated using the RK equation of state.

The transcritical depressurization phenomenon of supercritical carbon dioxide can be summarized into two types:

1. Single-Phase Transcritical Depressurization When the initial temperature is higher than the pseudo-critical temperature, the depressurization process maintains gaseous phase throughout without phase transition.

2. Phase-Transition Transcritical Depressurization When the initial temperature is lower than the pseudo-critical temperature, the fluid first depres-

surizes from the supercritical state into the saturation region, transitioning to liquid phase (gas-liquid two-phase depressurization). The saturated liquid then undergoes flash evaporation into gaseous state. With continued pressure reduction, the saturated liquid fully transitions to gas phase, resuming single-phase depressurization. If the temperature continues to drop during the flash evaporation process, liquid droplets solidify into dry ice [13]. After flash evaporation, CO_2 exists in both gas and solid phases.

The pseudocritical temperature is as shown in Eq. (1) [14]:

$$T_{pc} = -122.6 + 6.124p - 0.1657p^2 + 0.01773p^{2.5} - 0.0005608p^3,$$

where the pseudocritical temperature T_{pc} is in °C and the pressure p is in bar.

For the LBE-SCO_2 printed circuit heat exchanger, the system operates at 550-800 K with a cold-side working pressure of 20 MPa and hot-side at atmospheric pressure. During depressurization events within the 20 MPa range, the temperature consistently remains significantly above the pseudocritical temperature. Consequently, when boundary failure accidents occur, the supercritical CO_2 undergoes single-phase depressurization. Considering the nonlinear changes in the thermophysical properties of transcritical fluids, it is necessary to introduce real gas equations of state (EOS), such as SRK, PR and other equations of state, which provide high accuracy for the thermodynamic parameters of supercritical fluids [15].

In this paper, the optimal equation of state for transcritical CO_2 simulation is determined by numerical modeling and comparative analysis of experimental data. Meanwhile, the turbulence models commonly used in S-CO_2 CFD calculations, such as SST k-ω and SST k-ω low-Re [16], are mainly used for heat transfer analysis. Their applicability to transcritical depressurization conditions requires further validation. Therefore, the selection of turbulence models for the depressurization case is further investigated based on the selection of the equation of state. The main turbulence models in CFD currently include k- , k-ω, Reynolds stress, LES models, etc. Due to the poor convergence of the Reynolds stress model and the high computational cost of the LES model, as well as the unsuitability of the standard k- model for simulations involving near-wall flows, the selection is narrowed down to the k-ω model and other k- variants.

1. Numerical Simulation of CO_2 Depressurization in a Short Pipe

To verify the state equation and turbulence model, the experiments of Liu et al. [17] were selected. They conducted short-tube blowdown experiments with R744 refrigerant (CO_2) to investigate its transcritical flow characteristics. The experimental setup is illustrated in Fig. 2 [FIGURE:2]. The pipe has a length of 12.92 mm and an inner diameter of 1.35 mm. The copper tube diameter is 7 mm. Using pressure inlet and outlet as boundary conditions as shown in Table 1 , monitoring points were established to monitor the pressure as in the

experiment. Based on the inlet and outlet pressures, the specific heat capacities at 9.02 MPa, 6.3 MPa and 3.53 MPa were selected for calculation, as shown in Fig. 4 [FIGURE:4] and Fig. 5 [FIGURE:5]. It can be observed that the closer the properties are to the inlet conditions, the better the simulation matches the experimental values, regardless of the turbulence model or EOS selected. Therefore, this study defines the specific heat capacity based on the initial pressure.

The simulated values were compared with the experimental values and the maximum as well as average errors are shown in Table 2 . According to the error analysis, there was no significant difference between the four equations of state in this experimental simulation except for the ideal gas equation. This is because the ideal gas equation is not applicable to high temperature and pressure conditions. Among the four equations of state, the maximum and average errors of the PR and RK EOS are very small. Similarly, the turbulence model has little effect on this simulation. The simulation using SST k-ω low-Re and Realizable k- models are in good agreement with the experiment.

2. Numerical Simulation of CO_2 Depressurization in Vessel To further evaluate the applicability of the S-CO_2 equation of state and turbulence model, a different experiment from the short tube depressurization was chosen. This section presents simulation verification of the S-CO_2 vessel depressurization experiments conducted by Wang et al. [9]. Two of the experiment conditions were selected, and the experiment conditions are summarized in Table 3 . The experimental facility is shown in Fig. 8 [FIGURE:8].

Fig. 9 [FIGURE:9] shows the axisymmetric model. Fig. 10(a) and Fig. 10(b) [FIGURE:10] show the pressure variations calculated using the SST k-ω Low-Re turbulence model for different specific heat capacities. The results are consistent with the conclusions drawn in section II A 1: the closer to the initial state, the better the agreement with the experimental values. Further error analysis of the experimental and simulated values is shown in Table 4 and Table 5 . The variation of pressure over time with different nozzle sizes is shown in Fig. 11 [FIGURE:11] and Fig. 12 [FIGURE:12]. Based on the error analysis, for the turbulence model, regardless of the chosen equation of state (EOS), the SST k-ω Low-Re model demonstrates outstanding applicability in the transcritical depressurization of S-CO_2 simulation. In terms of the equation of state, the Peng-Robinson (PR) equation shows reliable performance across all tested turbulence models. Therefore, in this paper, the SST k-ω low-Re model is used as the turbulence model, and the PR equation of state is chosen for the thermophysical property calculation of S-CO_2.

It was found that the convergence of the k- model was inferior to that of the k-ω model, and the k- model was extremely prone to divergence under the same conditions, so only the k-ω model was used for the calculation. The same monitoring points as the experiment were established to monitor the pressure. Similarly, the specific heat capacity was tested under different pressures. The specific heat capacities at 8.1 MPa, 4.4 MPa and 0.1 MPa were selected for

calculation.

B. Validation of the Gas Injection Model for Liquid Metal

The SST k-ω low-Re turbulence model was selected for numerical simulation based on section II A 1. However, whether this turbulence model is suitable for studying pressure wave propagation in liquid metals still requires further verification. To assess the model's reliability, a gas injection experimental simulation was conducted. Currently, experiments on liquid lead-bismuth eutectic are more focused on lead-water reactions, while gas-liquid metal interaction experiments primarily focus on bubble dynamics. The injection of high-pressure water differs fundamentally from gas injection: water undergoes flash evaporation and phase change, whereas gas does not, leading to completely different pressure wave generation mechanisms.

For gas injection experiments, M. Utili et al. [18] conducted tests on helium gas impacting liquid lead-lithium (PbLi) to study IN-BOX LOCA, using Relap5 to analyze the propagation of pressure waves. Zhang et al. [19] investigated IN-BOX LOCA by injecting helium gas into liquid lead-lithium (PbLi) and performed pressure wave propagation analysis using Fluent [20]. To study the steam generator tube rupture (SGTR) of fast reactors, M V Alekseev et al. [21] used argon gas injection into Rose's alloy experiment to observe pressure wave dynamics.

As there are currently no experiments on the contact between supercritical carbon dioxide and liquid metal, this section selects the experiment of M V Alekseev et al. [21] for simulation to verify the correctness of the model. The test section and simulation model of the experiment are shown in Fig. 13 [FIGURE:13]. In this paper, the Mixture model with moderate accuracy and computational cost was chosen as the multiphase flow model.

In the selection of the drag force model, Zhang et al. [22] investigated the rising behavior of single bubbles in gallium indium tin alloy, and found that the Grace model and the Tomiyama model had smaller errors compared with the experimental values. Qing [23] simulated and analyzed the rising process of argon in gallium-indium-tin alloy, and found that the Tomiyama model showed better agreement with the experimental values. Chen [24] conducted numerical simulations of bubbles of different sizes rising in liquid lead. The results indicate that the Tomiyama model provides the best prediction for the terminal rising velocity of the bubbles. Thus, the Tomiyama model is selected as the trailing force model in Fluent.

Rose's metal consists of 50% bismuth, 25-28% lead and 22-25% tin by weight. The initial temperature of the experiment is 408 K, at atmospheric pressure. The argon gas injection pressure is 300 kPa, and the temperature is at room temperature. The Tait equation of state is used to describe the changes in density and sound speed of the liquid metal, as defined by the UDF, as shown in Eq. (2) and Eq. (3).

$$\rho = \rho_0 + \frac{1}{BS} \cdot (P - P_0)$$

$$c = \sqrt{\frac{BS}{\rho}}$$

where ρ is the current density, ρ_0 is the reference density, P is the current pressure, P_0 is the reference pressure, BS is the bulk modulus, and c is the local sound speed.

Pressure monitoring was conducted on sensor 1 as shown in Fig. 13 [FIGURE:13], and the calculated values by Fluent are shown in Fig. 14 [FIGURE:14]. Although there is a certain difference between the simulated values and the experimental values at the peak, the overall trend is consistent. Moreover, the simulation in this study is closer to the experimental values compared to the results by M V Alekseev et al. using OpenFoam [21]. Therefore, it can be concluded that the method in this study is capable of simulating the pressure wave analysis of liquid metal and gas contact. These models will be used in the simulation of the pressure boundary failure accident of PCHE.

III. SIMULATION MODELS

To simulate the potential pressure boundary failure accident of PCHE, the SUstainable Modular Mobile Enhanced Reactor (SUMMER) developed by the University of Science and Technology of China was used as the primary circuit [26]. Core design parameters are listed in Table 6 . The secondary circuit is a supercritical carbon dioxide Brayton cycle. The parameters of the printed circuit heat exchanger are shown in Table 7 , and the steady-state operation parameters of the PCHE heat exchange unit are provided in Table 8 .

When a pressure boundary failure accident occurs, it is assumed that the rupture occurs in the middle of the channel, and a straight-line crack forms, connecting the hot and cold channels through this crack. The cross-section of the rupture is a square with a side length of 0.1 mm, as shown in Fig. 17 [FIGURE:17]. Due to the short simulation time, the heat transfer between the hot and cold channels is neglected in this study. The solid domain is also ignored in the modeling, and the computational domain is shown in Fig. 18 [FIGURE:18].

IV. PRESSURE ANALYSIS OF PRESSURE BOUNDARY FAILURE ACCIDENTS IN PCHE

A. Grid Independence Verification

In this study, ICEM is employed for grid generation, with grids near the rupture zone encrypted to capture flow details. Since the primary focus is on observing pressure changes within the hot channel, its grid is further refined to enhance resolution. Pressure wave peak values at points A, B2, and C2 are selected for

comparative analysis as the grid number varies. Grid independence verification results are presented in Fig. 20 [FIGURE:20], showing that when the grid count reaches 860,000, the pressure peaks at all monitored points exhibit negligible variation with additional grid refinement. Consequently, this grid configuration is chosen for subsequent calculations, and the generated grid is visualized in Fig. 21 [FIGURE:21].

B. The Effect of Specific Heat Capacity on Pressure Waves

As concluded in the previous section, the density of S-CO_2 is described using the PR equation of state. The viscosity and thermal conductivity are calculated using bilinear interpolation, where the physical properties are interpolated based on both temperature and pressure as the two parameters and then imported through UDF. This section examines the effects of pressure-dependent specific heat capacity variations on pressure wave propagation. Pressure wave analysis of the specific heat capacity of point A and B2 was conducted at temperatures ranging from 550 K to 800 K under the conditions of 0.1 MPa, 10 MPa and 20 MPa, as shown in Fig. 22 [FIGURE:22] and Fig. 23 [FIGURE:23].

The results indicate that specific heat capacity variations under the three pressures have negligible effects on pressure wave propagation, with nearly identical trends and peak values. This is because the operating temperature is in the high-temperature range, far from the pseudo-critical region, thereby minimizing the pressure effect on specific heat capacity. Thus, this study uses the specific heat capacity at 20 MPa for calculations.

C. Pressure Analysis

Given that the sound speed in liquid lead-bismuth eutectic approaches 1900 m/s, pressure waves exhibit rapid propagation with short transit times. During boundary failure accidents, the most intense pressure wave dynamics occur in the initial stage, after which pressure gradually stabilizes over time. To ensure comprehensive observation of pressure wave propagation while managing computational costs, a long-time-scale simulation was first performed to identify the phase with the most intense pressure waves. Subsequently, short time-step simulations were conducted to characterize the fine-scale features of pressure wave propagation.

Monitoring the CO_2 volume fraction at points B and C, as shown in Fig. 26 [FIGURE:26], reveals that CO_2 starts to appear at point B around 0.001 s and at point C around 0.015 s, indicating CO_2 migration from the rupture to these locations. The pressure increase at this stage differs from the initial 0.001 s: it is not caused by the rupture-induced shockwave but rather by the gradual filling of the pipeline with released CO_2 gas, leading to pressure buildup.

1. Long Time Scale Simulation Fig. 24

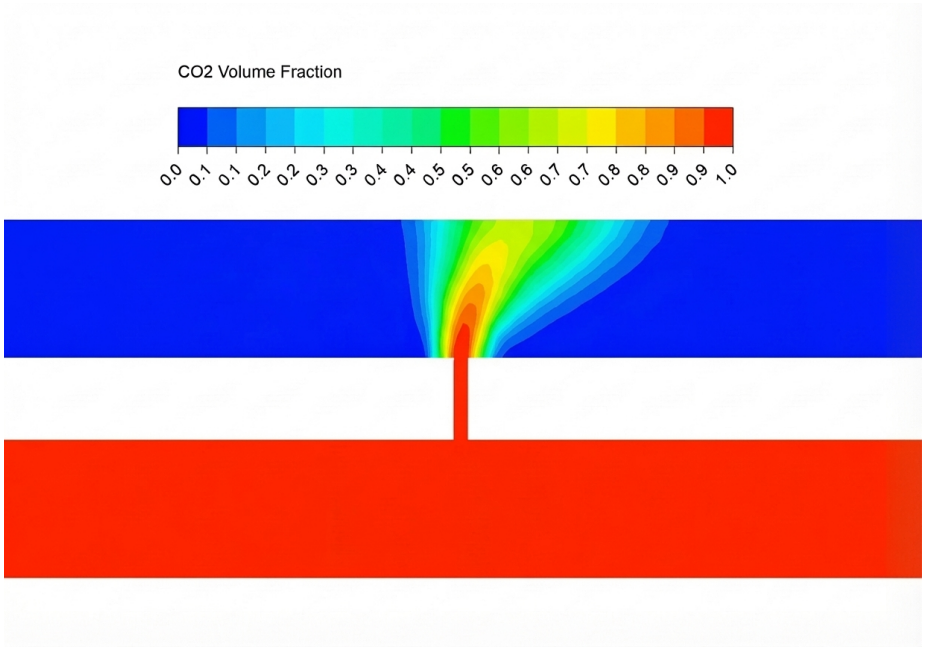

Figure 1: Figure 24

and Fig. 25 [FIGURE:25] are performed with a time step of 1E-04 s. The pressure wave undergoes the most significant changes during the first 0.001 s, after which the pressure gradually stabilizes. Starting at approximately 0.015 s, the pressure at points B and C gradually increases. For the CO_2 channel, pressure changes can be considered negligible, remaining close to the operating pressure of 20 MPa. This is because the properties of supercritical fluids lie between liquid and gas, allowing it to fill the entire channel like a gas, while also exhibiting the flow characteristics of a liquid, resulting in good expansion properties. When leakage occurs, the incoming CO_2 at the inlet rapidly compensates for the loss. Additionally, due to the high operating pressure of CO_2, pressure waves reflected back from the LBE channel are almost negligible.

The volume fraction of CO_2 at the hot channel inlet and outlet was monitored. As shown in Fig. 27 [FIGURE:27], CO_2 begins to appear at both locations after 0.015 s. Due to flow direction effects, the outlet exhibits CO_2 earlier than the inlet, indicating that flow-induced entrainment dominates over buoyancy-driven upward migration. Within the subsequent 0.02 s, the CO_2 volume fraction at both inlet and outlet rapidly increases to 90%, nearly filling the entire inlet and outlet. CO_2 completely fills the hot channel, demonstrating that during a PCHE boundary failure accident, CO_2 is highly likely to escape from the heat exchanger into the reactor system, posing a threat to reactor safety.

2. Short Time Scale Simulation Based on the long-timescale pressure wave analysis in the previous section, the most intense pressure wave variation occurs within the first 0.001 s after accident initiation. Consequently, in this section, a short time step is used to specifically analyze pressure wave propagation within 0.001 s. Long time scale calculations, compared to short time scale simulations as shown in Fig. 28 [FIGURE:28], omit many characteristics of pressure wave propagation, such as periodic pressure wave transmission phenomena analogous to shock tube behavior. The compression wave generated at the rupture propagates bidirectionally through the pipeline. Upon reaching the inlet and outlet boundaries, it reflects as expansion waves. These reflected expansion waves subsequently converge and superimpose at the pipeline's midsection, forming a higher-amplitude combined expansion wave. Following this interaction, the expansion waves separate and continue propagating toward the boundaries, where they reflect again as compression waves. These compression waves then converge centrally, completing one full cycle. This iterative process continues, with pressure waves reflecting and superimposing throughout the pipeline until complete attenuation is achieved.

As shown in Fig. 29 [FIGURE:29], the pressure wave reaches point B2 at 0.08 ms, and by 0.24 ms, it has returned, completing one cycle. The time interval from one peak to another is approximately 0.2 ms, and the propagation time is consistent with that of sound propagation in LBE. However, point A exhibits no pressure oscillations. This is because point A is positioned directly above the rupture point. After the pressure reaches its peak, CO_2 gas rapidly fills the pipeline in the vicinity of point A. Thereafter, the pressure exhibits a linear change, primarily due to the depressurization of CO_2.

Fig. 30 [FIGURE:30] illustrates the pressure evolution in the cold channel. Regardless of whether the simulation uses a long or short time scale, pressure wave variations within the cold channel remain minimal. After the accident occurs, the pressure in the cold channel starts to decrease, but the reduction is negligible, and the pressure remains nearly constant at the operating pressure of 20 MPa. Notably, the cold channel pressure also exhibits periodic variations: after 2-3 oscillations, the pressure gradually stabilizes. The period of this periodic variation is approximately 1 ms, and the sound speed in S-CO_2 is about 400 m/s, which matches the theoretical calculation results. For monitoring points that are symmetrically located around the crack, such as B1, B2, C1, and C2, their propagation characteristics are almost identical, with negligible influence from the direction of fluid flow. Although using long time-step simulation calculations can reduce computational effort, the accuracy in terms of characteristics such as the propagation of pressure waves and peak values is far less precise compared to short time-step simulations. However, for observing trend changes, such as the variation in gas fractions within the pipeline or changes in pressure waves, long time-step calculations can fully meet the computational requirements.

Monitoring the pressure at rupture point R, as shown in Fig. 31 [FIGURE:31], revealed a sharp pressure drop within 0.1 ms, followed by a stable period lasting

approximately 0.25 ms, after which another decline occurs and the pressure eventual stabilization at around 10 MPa. The duration of the first pressure stabilization phase is consistent with the transition period observed at point A.

Further analysis of the temperature and velocity at point R (as shown in Fig. 32 [FIGURE:32]) reveals that these parameters exhibit similar variation trends to those at point R. A comparison of pressure, temperature, and velocity at point R with the pressure at point A is shown in Fig. 33 [FIGURE:33]. Both points had a stable period prior to 0.25 ms. During the accident, the expansion of CO_2 could be divided into two types. Due to the rupture's perpendicular orientation relative to the flow path, supercritical carbon dioxide initially sprayed freely along the crack direction.

Fig. 34 [FIGURE:34] presents the CO_2 volume fraction distribution on the rupture plane perpendicular to the flow direction at 0.03 ms. At this stage, the flow velocity is approximately 250 m/s, which remains below the local speed of sound (under 14 MPa, 595 K conditions), and critical flow conditions are not yet achieved.

When the ejected CO_2 impacts the upper wall and is deflected, it fills the rupture plane and begins expanding laterally along the channel. Fig. 35 [FIGURE:35] shows the distribution of CO_2 volume fraction on the cross-sectional plane perpendicular to the flow direction at the breach location at 0.26 ms.

Fig. 36 [FIGURE:36] illustrates the CO_2 volume fraction distribution on the rupture plane parallel to the flow direction at 0.26 ms. The CO_2 expands laterally along both sides of the flow channel, and all subsequent CO_2 leakage from the rupture follows this expansion pattern. By 1 ms, the leakage velocity stabilizes at approximately 360 m/s. As shown in Fig. 33, the temperature remains steady around 560 K, and the pressure maintains at 10 MPa. At this stage, the leakage velocity reaches the local sound speed, signifying that the CO_2 flow has reached critical flow conditions. With continuous CO_2 replenishment from the cold channel inlet, the depressurization process will persistently proceed under critical flow conditions.

V. CONCLUSION

This study decouples the interaction characteristics between S-CO_2 and lead-bismuth eutectic into two distinct models: a transcritical depressurization model and a liquid metal-gas contact model. These models are verified through corresponding experiments to demonstrate the feasibility of simulating the pressure boundary failure accident of printed circuit heat exchangers. ANSYS Fluent is used to simulate the boundary condition failure accident of the PCHE, and an analysis of pressure wave propagation in the pipeline is conducted. The results are summarized as follows:

1. Through experimental validation, the Peng-Robinson (PR) equation of state demonstrates excellent applicability in simulating the transcritical

depressurization of S-CO_2.

2. Turbulence model selection is critical for accurate simulation of supercritical CO_2 transcritical depressurization. By comparing several mainstream CFD turbulence models with experiments, the SST k-ω low-Re model is shown to significantly enhance prediction accuracy for CO_2 transcritical depressurization behavior.

3. In the pressure boundary failure accident of printed circuit heat exchangers, the injection of high-pressure S-CO_2 into low-pressure lead-bismuth eutectic (LBE) generates shock wave effects within the pipeline. The pressure wave exhibits quasi-periodic oscillations, reaching almost 17 MPa within 0.1 ms after the accident occurs and then gradually decays. By 10 ms, leaked CO_2 begins to fill the entire hot channel, causing renewed pressure rise due to CO_2 migration. At 30 ms, CO_2 concentration at the inlet/outlet reaches nearly 90%, indicating potential leakage into the reactor system.

This study focuses on the simulation of pressure boundary failure accidents for a single rupture size. Further investigation is required to examine the effects of varying rupture dimensions on accident progression, as well as the influence of rupture location on pressure wave dynamics and CO_2 migration within the pipeline. Additionally, the observed pressure wave characteristics exhibiting high peak magnitudes but short duration may induce structural failure in the heat exchanger. Stress analysis is required to assess the structural impact. These aspects need to be further researched in future studies.

REFERENCES

[1] Pioro, I.L., Introduction: Generation Iv International Forum. HANDBOOK OF GENERATION IV NUCLEAR REACTORS, 2016.

[2] Dawei, C., S. Lei and L. Jiming, Study on coupling heat transfer model and characteristics of supercritical carbon dioxide and liquid lead-bismuth eutectic. THERMAL POWER GENERATION, 2022. 51(6): p. 59-67.

[3] Yike, N., et al., A review of lead-bismuth supercritical CO2 heat transfer in lead-bismuth fast reactor-supercritical CO2 cycle system. Electric Power Technology and Environmental Protection, 2023. 39(6): p. 471-483.

[4] Eoh, J., et al., Potential sodium–CO2 interaction of a supercritical CO2 power conversion option coupled with an SFR: Basic nature and design issues. Nuclear Engineering and Design, 2013. 259: p. 88-101.

[5] Kisohara, N., Y. Sakamoto and S. Kotake, Preliminary Conceptual Design of the Secondary Sodium Circuit-Eliminated JSFR (japan Sodium Fast Reactor) Adopting a Supercritical CO2 Turbine System, 1; Sodium/CO2 Heat Exchanger. 2014. 214: p. 1-33.

[6] Jintao, L., et al., Corrosion Behavior of Alloys in Supercritical CO2 Brayton Cycle Power Generation. Proceedings of the CSEE, 2016. 36(3): p. 739-745.

[7] Kang, L., The physical mechanism of the supercritical CO2 leakage process in small scale laboratory conditions.. 2016, University of Science and Technology of China.

[8] Gebbeken, B. and R. Eggers, Blowdown of carbon dioxide from initially supercritical conditions. Journal of loss prevention in the process industries, 1996. 9(4): p. 285-293.

[9] Wang, J., et al., Study on Factors Affecting During Carbon Dioxide Vessel Decompression at Supercritical Pressure. Nuclear Science and Technology, 2021. 09: p. 29-37.

[10] Guo, X., et al., Pressure responses and phase transitions during the release of high pressure CO2 from a large-scale pipeline. Energy, 2017. 118: p. 1066-1078.

[11] Yang, M., et al., Characteristic Analysis and Model Validation of Supercritical Carbon Dioxide Ejection in Pressure Vessel. Atomic Energy Science and Technology, 2023. 57(7): p. 1363-1372.

[12] Feng, L., Study on the leakage and diffusion behavior of supercritical pressure CO2 from pipelines. 2016, Tsinghua University.

[13] Woolley, R.M., et al., Experimental measurement and Reynolds-averaged Navier-Stokes modelling of the near-field structure of multi-phase CO2 jet releases. International Journal of Greenhouse Gas Control, 2013. 18: p. 139-149.

[14] Liao, S.M. and T.S. Zhao, Measurements of Heat Transfer Coefficients From Supercritical Carbon Dioxide Flowing in Horizontal Mini/Micro Channels. Journal of Heat Transfer, 2002. 124(3): p. 413-420.

[15] Ribert, G., et al., Simulation of supercritical flows in rocket-motor engines: application to cooling channel and injection system. Progress in Propulsion Physics 4, 2013: p. 205-226.

[16] Xianliang, L., et al., Research progress on conjugated heat transfer between supercritical carbon dioxide and liquid metals. THERMAL POWER GENERATION, 2023. 52(6): p. 1-11.

[17] Liu, J.P., et al., Experimentation and correlation of R744 two-phase flow through short tubes. Experimental Thermal and Fluid Science, 2004. 28(6): p. 565-573.

[18] Utili, M., et al., THALLIUM: An experimental facility for simulation of HCLL In-box LOCA and validation of RELAP5-3D system code. Fusion Engineering and Design, 2017. 123: p. 214-221.

[19] Shichao, Z., et al., Pressure Propagation Experiments of PbLi Impacted by High Pressure Helium under the Condition of Fracture. Nuclear Science and

Engineering, 2019. 39(6): p. 678-689.

[20] Shichao, Z., Transient Study of In-box LOCA in Dual-functional Lead Lithium Blanket. 2020, University of Science and Technology of China.

[21] Alekseev, M.V., et al., Numerical simulation of pulsed gas-to-liquid injection modes using open source CFD software package OpenFoam. Journal of physics. Conference series, 2018. 1105(1): p. 12085.

[22] ZHANG C, ECKERT S, GERBETH G. The flow structure of a bubble-driven liquid-metal jet in a horizontal magnetic field[J]. Journal of Fluid Mechanics, 2007,575:57-82.

[23] Chong, Q., Numerical Simulation and Analysis of Steam Generator Tube Rupture Accident of Straight Tube Heat Exchanger in Lead-cooled Fast Reactor. 2024, University of Science and Technology of China.

[24] Jiaming, C. and C. Hongli, Void Transport after Steam Generator Tube Leakage in Natural Circulation Lead-cooled Fast Reactor. Atomic Energy Science and Technology, 2020. 54(12): p. 2344-2352.

[25] Usov, E.V., et al., Experimental and numerical simulation of gas bubbles motion in liquid metal. Journal of physics. Conference series, 2018. 1128(1): p. 12044.

[26] Kefan. Z., et al., SUMMER: A small modular lead-bismuth-cooled fast reactor for mobile energy supply. Progress in Nuclear Energy, 2023. 164: p. 104860.